

Non-equilibrium THz-phonon spin coupling in CrI₃

V Shokeen¹, M Pavelka¹, R Chulkov¹, A Yaroslavtsev^{1,2}, J Rogvall¹, D Muradas Belinchón¹, U Noumbe¹, M Abdel-Hafiez¹, M Venkata Kamalakar¹, O Grånäs¹ and H A Dürr¹

¹Department of Physics and Astronomy, Uppsala University, Uppsala, Sweden

²MAX IV Laboratory, Lund University, Lund, Sweden

E-mail: vishal.shokeen@physics.uu.se

Abstract. Manipulating magnetism at the THz timescale in atomically thin ferromagnets by exploiting the interactions of spins with optical phonon modes presents an innovative idea for THz spintronics. Spin-phonon coupling raises an important question about the flow of spin angular momentum possibly to chiral phonons. We use femtosecond optical pulses to generate bound electron-hole pairs (excitons) in the 2D ferromagnet CrI₃, and probe the subsequent charge and spin dynamics. The observed change in the optical signal during temporal pump-probe overlap represents the buildup of the exciton population. This is accompanied by the excitation of coherent optical phonon modes with 2.4 and 3.9 THz frequencies, corresponding to the bending and stretching of the Cr-I bonds. We observe both modes in the magnetism channel which agrees with first-principles calculations that identify changes in the exchange coupling due to the lattice displacements for both phonon modes.

1. Introduction

The fundamental interaction between atomic structure and magnetic ordering undoubtedly provides a versatile tool to control the properties of materials. Manipulating electron spins via phonons or vice-versa opens the path for controlling magnetic or structural phase transitions. An important and pertinent question is the mechanism for the conservation of angular momentum between spins and lattice/phonons which has transpired as the Einstein de-Haas [1] and Barnett effects [2]. This coupling potentially plays a consequential role in the motion of domain walls [3], the polarization of phonons [4], magnetic switching in a mechanical nano-cantilever [3], superconductivity [5], spin relaxation in molecular magnets [6], negative thermal expansion [7] etc. At the same time, light-matter interaction at ultrafast timescales in dimensionally confined systems is an intriguing subject for condensed matter research with enormous application potential [8] and exciting unconventional physics to be uncovered [9]. With the development of ultrashort laser pulses, this manipulation could be achieved and detected at ultrafast timescales which likely results in all-optical magnetic switching [10]. Magnetic van-der Waals systems intrinsically show strong coupling between different degrees of freedom, including spin and lattice projecting [11] themselves as an ideal platform to understand

the underlying mechanisms. Hence, it becomes vital to understand the microscopic mechanism for the spin-phonon interaction at its intrinsic timescales.

CrI₃ is a prototypical semiconducting ferromagnet with the T_c of 61 K in the bulk [12]. The electronic structure of CrI₃ is characterized by excitonic and charge transfer transitions [13,14] with strong electron-phonon [15] and magneto-optical coupling [13,16]. The individual layers of CrI₃ consist of a hexagonal lattice of Cr ions surrounded by iodine in octahedral geometry [13]. The Cr magnetic moment has been determined to be 3 μ_B with an out-of-plane magnetic anisotropy [13]. The magnetic ordering in 2D systems can overcome the constraints of Mermin-Wagner theorem [17] with strong magnetic anisotropy [18]. The magnetic anisotropy in CrI₃ is attributed to the superexchange interaction between Cr ions via the intermediate I ligand atoms [18] of the Cr-I bond, making it an active platform for diverse perturbation methods to modulate the magnetism of the semiconductor.

CrI₃ exhibits several optical phonon modes in the THz frequency range, however, their effect on the magnetic order remains ambiguous. The excitation of 2.4 and 3.9 THz frequency modes in CrI₃ has been observed with Raman scattering [19,20]. Additional phonon modes were reported to be excited through polaron formation [15]. Optically induced exciton formation was observed to lead to coherent excitation of the 2.4 and 3.9 THz phonon modes with time-resolved optical spectroscopy [14,21]. Polarized Raman scattering of these two modes has been interpreted to be due to magnon modes [19] but was subsequently shown to be caused by backfolded phonons [20]. Using optical pump-probe experiments, it was demonstrated that helicity-dependent optical excitation can affect the phonon mode population. However, only the 3.9 THz mode was reported to couple to the magnetic order [21].

In this article, we report the charge and spin dynamics in CrI₃ following exciton formation. The optical generation of excitons in CrI₃ is accompanied by a Jahn Teller-like lattice distortion that excites dispersive Raman-active phonon modes of A_{1g} and A_{2g} symmetry at 2.4 and 3.9 THz, respectively [14]. We show, using the magneto-optical Kerr effect (MOKE), that both modes couple to the magnetic order. Ab-initio calculations demonstrate that both modes change the magnetic exchange parameters.

2. Results and discussion

We used time-resolved optical and magneto-optical Kerr spectroscopy to investigate the charge and spin dynamics in CrI₃. Bulk crystal of CrI₃ was exfoliated as flakes onto a SiO₂/Si substrate and transferred into an LHe cryostat in the Ar atmosphere.

Subsequently, measurements were performed in vacuum in the cryostat, circumventing the corrosion of the air-sensitive samples. The samples were excited with linearly p-polarized 1.57 eV pump and probed with photon energy of 2.4 eV. The pump and probe laser pulses were focused to 40 and 10 μm, respectively, onto the CrI₃ flakes of ~70 μm size. The incidence angle of the p-polarized pump and p-polarized probe beams were ~0° and ~22° relative to the sample normal, respectively. The overall temporal resolution given by the convolution of pump and probe pulses was 200±5 fs. The measurements were performed at a sample temperature of 4 K under applied out-of-

plane magnetic fields of ± 0.3 T. The pump-probe time delay ranges shown here were 5 ps with a step size of 25 fs. Time-resolved changes in reflectivity and magnetism were determined by the average change of the reflected probe intensity and the difference in polarization rotation for two opposite magnetic field directions ($\pm H$), respectively. The transient change in reflectivity and magnetism are normalized to the unpumped static values of the corresponding parameter.

Figure 1 shows the measured transient changes in the reflectivity ($\Delta R/R$) and MOKE rotation ($\Delta M/M$) vs. pump-probe time delay (symbols) for different pump fluences. The signal, $\Delta R/R$, measures changes in the electronic properties of the sample, while the magnetic Kerr rotation changes, $\Delta M/M$, are directly related to the magnetic properties. Both $\Delta R/R$ and $\Delta M/M$ display an initial decrease followed by a slow recovery in the $\Delta R/R$ -channel and a further decrease in the $\Delta M/M$ -channel. The dynamics after the initial decrease is also accompanied by coherent oscillations. In order to extract the size of the coherent oscillations, we model the initial signal drop and further dynamics averaged over the coherent oscillations by the functional form shown in Eq. (1)

$$\frac{\Delta Z}{Z} = A(t) \frac{\Delta Z_{Ex}}{Z} \left\{ 1 + \Delta Z_{ps} \left(1 - e^{-\frac{(t-t_0)}{\tau_Z}} \right) \right\} \quad \text{Eq. (1)}$$

with $Z = R$ or M , describing the reflectivity and magnetism data, respectively. In Eq. (1), we describe the initial signal drop by the normalized integral over the pump-probe pulse convolution, $A(t)$ multiplied by the size of the drop, $\frac{\Delta Z_{Ex}}{Z}$, due to exciton formation and its temporal full width at half maximum, τ_{fwhm} , as fit parameters. The subsequent ps dynamics is modeled by an exponential recovery in R and a decay in M , with amplitudes, ΔZ_{ps} and timescales, τ_Z , for R and M , respectively. We note that a continuing decay of M after the initial drop was also observed in ref. [21] and was assigned to ps demagnetization. All fit parameters are summarized in Table 1 for reflectivity, R , and in Table 2 for magnetism, M .

The initial signal drops observed in Fig. 1 show a width that varies significantly less than the temporal step size of the measurements, i.e. the width is essentially constant for R and M at all pump fluences. The time width of the drop, τ_{fwhm} , is estimated from Eq. (1) to be 200 ± 5 fs which agrees with the temporal convolution of pump probe pulses. We use the fitted maxima of pump-probe convolution to determine the time zero positions of the time delay axes in Fig. 1. The size of the initial drop scales linearly with pump fluence, as shown in the inset of Fig. 1. This is the expected behavior for exciton generation being the responsible mechanism since each exciton generated has to absorb the same number of photons regardless of the incident fluence. Only for high exciton densities can exciton-exciton interaction lead to a non-linear behavior [14]. This is, however, not observed within our fluence range. We finally note that the subsequent system evolution can systematically influence the parameters extracted for the initial drop. With increasing pump fluence this is mainly due to the appearance of coherent oscillations which will be discussed in the following.

After the initial drop of $\Delta M/M$ and to a lesser degree of $\Delta R/R$, coherent oscillations are observed (see Fig. 1). Here, we focus on the coherent phonons visible in the magnetic signal. Results are analyzed and shown in Fig. 2 after subtracting the background $\Delta M/M$ signal according to Eq. (1).

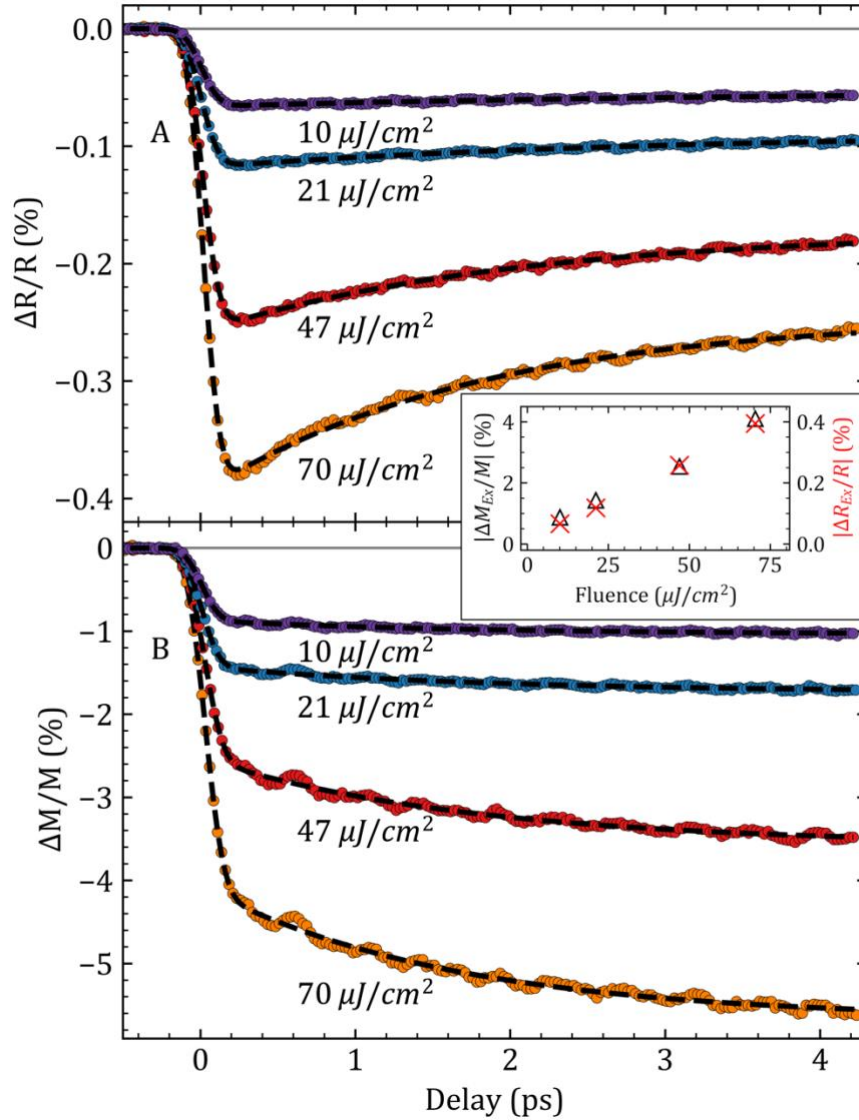


Figure 1. Ultrafast reflectivity (A) and magnetization dynamics (B) of CrI_3 for different pump fluences stated in the figure. Symbols are the experimental data and dashed lines describe the fit according to Eq. (1), as discussed in the text. The inset displays the fluence dependence of the absolute values of the initial signal drop in R (red crosses) and M (black open triangles) channels. The fit parameters are summarized in Tables 1 and 2 for R and M channels, respectively.

Similar oscillations have been observed in ref. [14] for R above the magnetic ordering temperature and for M in ref. [21]. The Fourier transforms of the coherent phonon

oscillations in refs. [14,21] show two peaks at 2.4 and 3.9 THz. In addition, the time-delay data in refs. [21] have been fitted to the superposition of sinusoidal functions at the two frequencies. Due to our restricted time-delay range, we use the time domain approach.

Table 1. Fit parameters for reflectivity data as estimated using Eq. (1)

Fluence ($\mu\text{J}/\text{cm}^2$)	$\Delta R_{\text{Ex}}/R$ (%)	ΔR_{ps} (%)	τ_{R} (ps)	τ_{fwhm} (ps)
70	-0.394	-0.379	1.8	0.197
47	-0.258	-0.332	2.0	0.204
21	-0.118	-0.246	2.9	0.208
10	-0.066	-0.196	3.3	0.210

Table 2. Fit parameters for magnetism data as estimated using Eq. (1)

Fluence ($\mu\text{J}/\text{cm}^2$)	$\Delta M_{\text{Ex}}/M$ (%)	ΔM_{ps} (%)	τ_{M} (ps)	τ_{fwhm} (ps)
70	-4.099	-0.383	1.6	0.222
47	-2.539	-0.406	1.7	0.225
21	-1.428	-0.214	1.8	0.213
10	-0.871	-0.192	1.7	0.209

Figure 2 shows the fit of the measured coherent oscillations observed in M for various pump fluences. The fit function $f(t)$ takes the amplitudes, A , frequencies, ν , and phases, ϕ , of both 2.4 THz and 3.9 THz modes into account as

$$f(t) = A_{2.4\text{THz}} \sin(\nu_{2.4\text{THz}} t + \phi_{2.4\text{THz}}) + A_{3.9\text{THz}} \sin(\nu_{3.9\text{THz}} t + \phi_{3.9\text{THz}}). \quad \text{Eq. 2}$$

In all cases, the measured oscillations are well reproduced by the fits (solid lines in Fig. 2) for delay times longer than ~ 1 ps. At earlier times larger oscillations than that the fits (dashed lines in Fig. 2) are observed. We note that upon approaching time-zero the initial signal drop due to exciton formation strongly affects the extracted oscillation amplitude. The fit parameters obtained for delay times longer than 1 ps are summarized in Table 3.

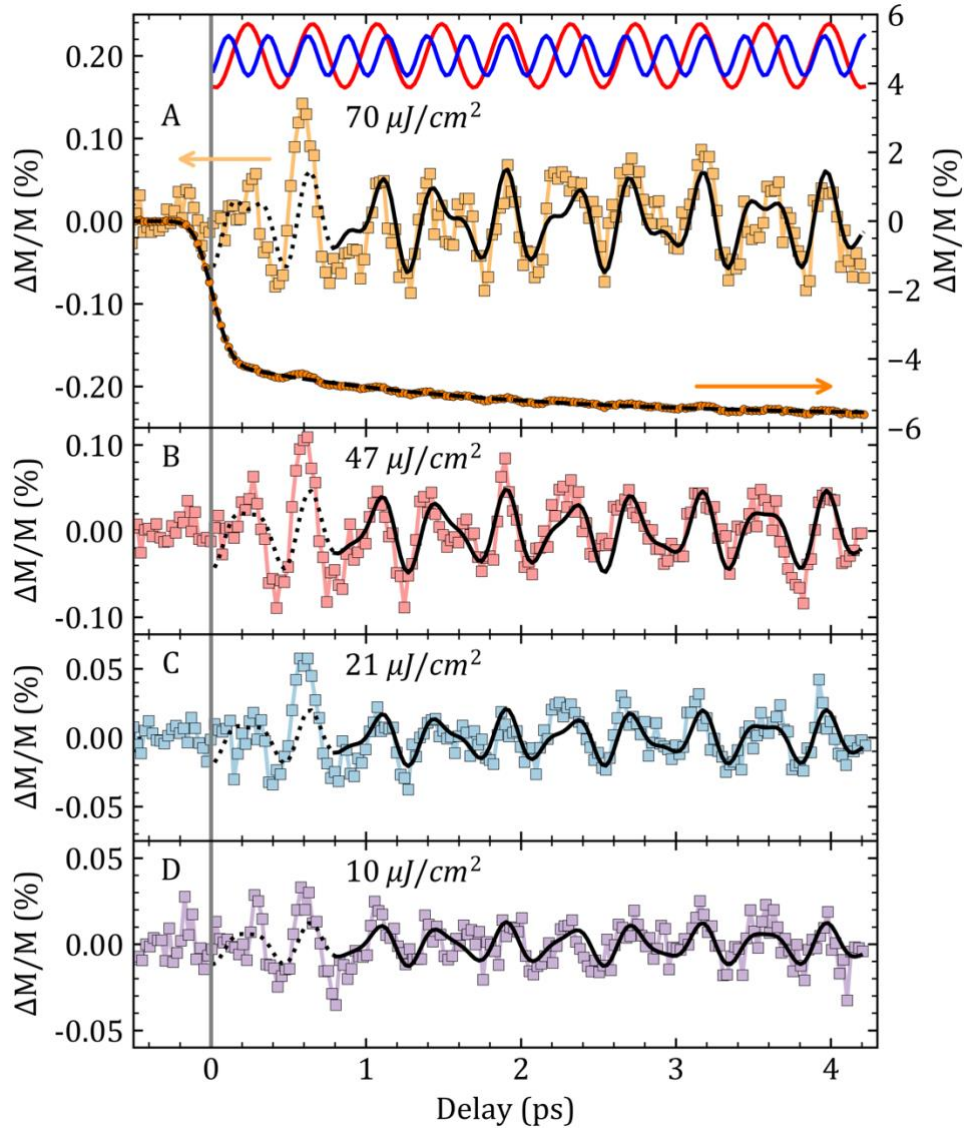


Figure 2. Coherent oscillations in the magnetic signal for different fluences. The oscillatory component of the magnetic signal is retrieved by removing the smooth background according to Eq. (1) from the measured $\Delta M/M$ signals, as shown in (A). The red and blue oscillations in (A) are the individual contributions of the 2.4 and 3.9 THz modes to the coherent oscillations in the magnetic signal. Experimental $\Delta M/M$ values due to the coherent oscillations are shown as colored lines and symbols. Fits according to Eq. (2) are shown as black solid lines, while the dotted black line is the extrapolation to $t=0$ for the visualization of the phase. The fit parameters are summarized in Table 3.

Figure 3 displays the fluence dependence of both phonon amplitudes in magnetism. They increase linearly with fluence. This indicates that their strength scales with the number of generated excitons. We choose to fix the phases for 2.4 THz and 3.9 THz modes to -2.0 and -1.2 radian respectively, corresponding to the values obtained for the highest pump fluence where the largest oscillation amplitudes are generated.

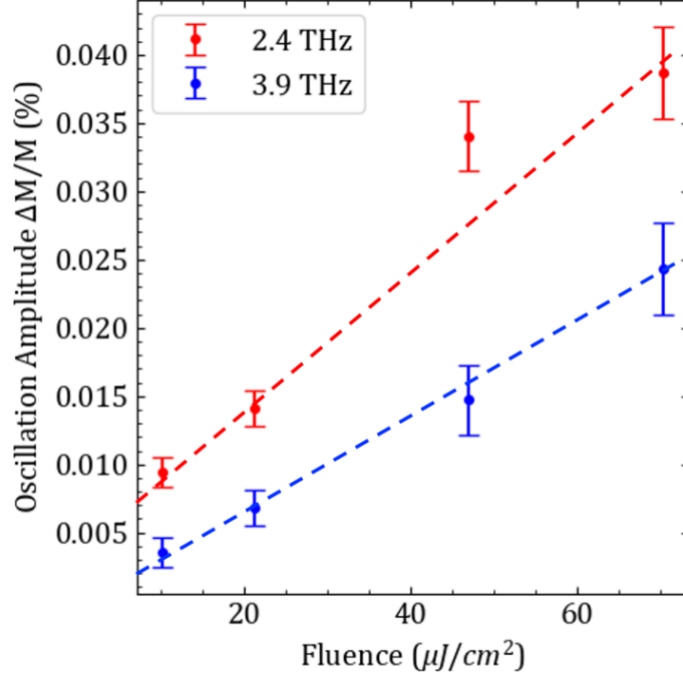


Figure 3. Fluence dependence of the amplitude of the coherent vibrational modes. a) The amplitude of 2.4 (red markers) and 3.9 (blue markers) THz as a function of the pump fluence. The amplitude of both modes increases linearly with the fluence as indicated by the red and blue dashed lines. The phase of the two modes is kept constant which is determined for the highest fluence.

Table 3. Amplitudes of two modes with 2.4 ($A_{2.4\text{THz}}$) and 3.9 ($A_{3.9\text{THz}}$) THz frequency for different fluences. The amplitudes are estimated using the Eq. (2).

Fluence($\mu\text{J}/\text{cm}^2$)	$A_{2.4\text{THz}}$ (%)	$A_{3.9\text{THz}}$ (%)
70	0.039	0.024
47	0.035	0.015
21	0.015	0.008
10	0.009	0.004

The two phonon modes have been identified as the bending and stretching of Cr-I bonds [14,20,21] for 2.4 and 3.9 THz, respectively. In order to understand their coupling to the magnetic order, we calculated the effective Heisenberg exchange in a supercell of 2x2x2 unit cells. The influence on the effective exchange coupling J_{eff} of each phonon-mode may, to first order, be estimated from the total energy of the ferro- and antiferromagnetic configurations under finite displacement of the optical phonon

modes. We find that for all Raman active modes the A_{1g} and A_{2g} modes at 2.4 THz and 3.9 THz, respectively, influence J_{eff} most. This allows us to visualize that we observe both modes in the magnetic channel in an amplified way, while they are essentially absent in reflectivity that probes their coupling to the electron charges.

3. Conclusion

We showed ultrafast laser-generated excitons inducing spin and charge dynamics in semiconducting 2D ferromagnet CrI_3 . The spin dynamics here differs from the usual ultrafast demagnetization induced by electronic heating. More importantly, the lattice undergoes a distortion due to the laser-excited bound e-h pair accompanied by the coherent vibrational modes. These vibrational modes with frequencies of 2.4 and 3.9 THz are the optical phonon modes that modulate the spin dynamics coherently. By combining experimental results and ab-initio simulations, we conclude that both 2.4 and 3.9 THz modes, corresponding to the bending and stretching of the Cr-I bonds, couple to the magnetism by modifying the exchange interaction.

Acknowledgement

V.S., M.P., J.R. and H.A.D. acknowledge support by the Swedish Research Council (VR 2022-02881) and the Knut and Alice Wallenberg Foundation (KAW). D.M.B. and M.V.K. gratefully acknowledge funding from the European Research Council (ERC) Project SPINNER (Grant No. 101002772) and Knut and Alice Wallenberg Foundation (Grants No. 2022.0079 and 2023.0336). O.G. Acknowledges financial support from the Swedish Research Council (VR) through grant 2019-0390 and European Research Council through the Synergy Grant 854843 – FASTCORR.

References

- [1] Einstein A and de Haas W J 1915 Experimenteller Nachweis der Ampèreschen Molekularströme *Deutsche Physikalische Gesellschaft* **17** 152–70
- [2] Barnett S J 1915 Magnetization by Rotation *Phys. Rev.* **6** 239–70
- [3] Jaafar R, Chudnovsky E M and Garanin D A 2009 Dynamics of the Einstein–de Haas effect: Application to a magnetic cantilever *Phys. Rev. B* **79** 104410
- [4] Tauchert S R, Volkov M, Ehberger D, Kazenwadel D, Evers M, Lange H, Donges A, Book A, Kreuzpaintner W, Nowak U and Baum P 2022 Polarized phonons carry angular momentum in ultrafast demagnetization *Nature* **602** 73–7
- [5] Keimer B, Kivelson S A, Norman M R, Uchida S and Zaanen J 2015 From quantum matter to high-temperature superconductivity in copper oxides *Nature* **518** 179–86
- [6] Kragoskow J G C, Mattioni A, Staab J K, Reta D, Skelton J M and Chilton N F 2023 Spin–phonon coupling and magnetic relaxation in single-molecule magnets *Chem. Soc. Rev.* **52** 4567–85

- [7] Kozlenko D P, Lis O N, Kichanov S E, Lukin E V, Belozerova N M and Savenko B N 2021 Spin-induced negative thermal expansion and spin–phonon coupling in van der Waals material CrBr₃ *npj Quantum Mater.* **6** 1–5
- [8] Dayen J-F, Ray S J, Karis O, Vera-Marun I J and Kamalakar M V 2020 Two-dimensional van der Waals spinterfaces and magnetic-interfaces *Applied Physics Reviews* **7** 011303
- [9] Wang Q H, Bedoya-Pinto A, Blei M, Dismukes A H, Hamo A, Jenkins S, Koperski M, Liu Y, Sun Q-C, Telford E J, Kim H H, Augustin M, Vool U, Yin J-X, Li L H, Falin A, Dean C R, Casanova F, Evans R F L, Chshiev M, Mishchenko A, Petrovic C, He R, Zhao L, Tsen A W, Gerardot B D, Brotons-Gisbert M, Guguchia Z, Roy X, Tongay S, Wang Z, Hasan M Z, Wrachtrup J, Yacoby A, Fert A, Parkin S, Novoselov K S, Dai P, Balicas L and Santos E J G 2022 The Magnetic Genome of Two-Dimensional van der Waals Materials *ACS Nano* **16** 6960–7079
- [10] Zhang P, Chung T-F, Li Q, Wang S, Wang Q, Huey W L B, Yang S, Goldberger J E, Yao J and Zhang X 2022 All-optical switching of magnetization in atomically thin CrI₃ *Nat. Mater.* **21** 1373–8
- [11] Hu L, Du K, Chen Y, Zhai Y, Wang X and Xiong Q 2023 Spin-phonon coupling in two-dimensional magnetic materials *NSO* **2** 20230002
- [12] Ghosh A, Jönsson H J M, Mukkattukavil D J, Kvashnin Y, Phuyal D, Thunström P, Agåker M, Nicolaou A, Jonak M, Klingeler R, Kamalakar M V, Sarkar T, Vasiliev A N, Butorin S M, Eriksson O and Abdel-Hafiez M 2023 Magnetic circular dichroism in the d d excitation in the van der Waals magnet CrI₃ probed by resonant inelastic x-ray scattering *Phys. Rev. B* **107** 115148
- [13] Wu M, Li Z, Cao T and Louie S G 2019 Physical origin of giant excitonic and magneto-optical responses in two-dimensional ferromagnetic insulators *Nature Communications* **10** 2371
- [14] Li X, Wang A, Chen H, Tao W, Chen Z, Zhang C, Li Y, Zhang Y, Shang H, Weng Y-X, Zhao J and Zhu H 2022 Ultrafast Spontaneous Localization of a Jahn-Teller Exciton Polaron in Two-Dimensional Semiconducting CrI₃ by Symmetry Breaking *Nano Lett.* **22** 8755–62
- [15] Jin W, Kim H H, Ye Z, Ye G, Rojas L, Luo X, Yang B, Yin F, Horng J S A, Tian S, Fu Y, Xu G, Deng H, Lei H, Tsen A W, Sun K, He R and Zhao L 2020 Observation of the polaronic character of excitons in a two-dimensional semiconducting magnet CrI₃ *Nat Commun* **11** 4780
- [16] Huang B, Clark G, Navarro-Moratalla E, Klein D R, Cheng R, Seyler K L, Zhong D, Schmidgall E, McGuire M A, Cobden D H, Yao W, Xiao D, Jarillo-Herrero P and Xu X 2017 Layer-dependent ferromagnetism in a van der Waals crystal down to the monolayer limit *Nature* **546** 270–3

- [17] Mermin N D and Wagner H 1966 Absence of Ferromagnetism or Antiferromagnetism in One- or Two-Dimensional Isotropic Heisenberg Models *Phys. Rev. Lett.* **17** 1133–6
- [18] Kim D-H, Kim K, Ko K-T, Seo J, Kim J S, Jang T-H, Kim Y, Kim J-Y, Cheong S-W and Park J-H 2019 Giant Magnetic Anisotropy Induced by Ligand L S Coupling in Layered Cr Compounds *Phys. Rev. Lett.* **122** 207201
- [19] Jin W, Kim H H, Ye Z, Li S, Rezaie P, Diaz F, Siddiq S, Wauer E, Yang B, Li C, Tian S, Sun K, Lei H, Tsen A W, Zhao L and He R 2018 Raman fingerprint of two terahertz spin wave branches in a two-dimensional honeycomb Ising ferromagnet *Nat Commun* **9** 5122
- [20] McCreary A, Mai T T, Utermohlen F G, Simpson J R, Garrity K F, Feng X, Shcherbakov D, Zhu Y, Hu J, Weber D, Watanabe K, Taniguchi T, Goldberger J E, Mao Z, Lau C N, Lu Y, Trivedi N, Valdés Aguilar R and Hight Walker A R 2020 Distinct magneto-Raman signatures of spin-flip phase transitions in CrI₃ *Nat Commun* **11** 3879
- [21] Padmanabhan P, Buessen F L, Tutchton R, Kwock K W C, Gilinsky S, Lee M C, McGuire M A, Singamaneni S R, Yarotski D A, Paramakanti A, Zhu J-X and Prasankumar R P 2022 Coherent helicity-dependent spin-phonon oscillations in the ferromagnetic van der Waals crystal CrI₃ *Nat Commun* **13** 4473